Conference paper

Amin Ismael, Manabu Abe, Rui Fausto* and Maria L. S. Cristiano*

Insights into the photochemistry of 5-aminotetrazole derivatives with applications in coordination chemistry. Effect of the saccharyl moiety on the photostability

Abstract: The properties and applications of 2-methyl-(2*H*)-tetrazole-5-amino-saccharinate (**2MTS**) in catalysis and chelant-based chemotherapy stimulated investigations on its photostability. The photochemistry of monomeric **2MTS** in solid argon (15 K) was compared with those of 2-methyl-(2*H*)-tetrazole-5-amine (**2MT**) and 1-methyl-(2*H*)-tetrazole-5-amine (**1MT**). Compounds were subjected to *in situ* narrowband UV-irradiation at different wavelengths. Reactions were followed by infrared spectroscopy, supported by B3LYP/6-311++G(d,p) calculations. Photochemical pathways for **2MT** and **2MTS** proved similar but photodegradation of **2MTS** was 20× slower, unraveling the photostabilizing effect of the saccharyl moiety that extends into the nitrilimine formed from **2MTS** and its antiaromatic 1*H*-diazirene isomer, which proved photostable at 290 nm, unlike the 1*H*-diazirene formed from **2MT**. Analysis of the photochemistries of **2MTS**/**2MT** (250 nm) and **1MT** (222 nm), including energy trends calculated for the isomeric $C_2H_5N_3$ species postulated/observed from photolysis and EPR results, enabled a deeper insight into the photodegradation mechanisms of 1,5-substituted and 2,5-substituted tetrazoles. We postulate a pivotal singlet state imidoylnitrene species, **ˢN1**, as common intermediate, which undergoes a Wolff-type isomerization to a stable carbodiimide. Photo-extrusion of N_2 from 1,5-substituted tetrazoles generates **ˢN1** directly but from 2,5-substituted tetrazoles it originates a nitrilimine, then a diazirene, which finally leads to **ˢN1**. Selective formation of cyanamide from **1MT** requires photoisomerization between **ˢN1** and **ˢN2**, accessible at 222 nm. EPR studies enabled the detection of methyl nitrene, arising from photolysis of 1*H*-diazirene intermediate.

Keywords: 5-aminotetrazoles; ICPOC-24; light-induced selectivity; photocleavage mechanisms; reactive intermediates; substituent effects; tetrazole-saccharinates.

Introduction

Tetrazoles exhibit excellent coordination abilities through their four nitrogen atoms, acting either as multidentate ligands or as bridging building blocks in supramolecular assemblies [1–4]. Additionally, the structure of the tetrazolyl-based coordination complexes can be tailored by employing functionalysed tetrazoles in the assembly process [5], increasing the versatility and widening the applications of the tetrazole chemotype in coordination and supramolecular chemistry. Likewise, benzisothiazoles (known as saccharins) bear

---

---

*Corresponding authors: Rui Fausto, Departmento de Química, Faculdade de Ciências e Tecnologia Universidade de Coimbra, Rua Larga, P-3004-535 Coimbra, Portugal; and CQC, Department of Chemistry, University of Coimbra, P-3004-535 Coimbra, Portugal, e-mail: rfausto@ci.uc.pt; and **Maria L. S. Cristiano,** Departamento de Química e Farmácia, Faculdade de Ciências e Tecnologia, Campus de Gambelas, Universidade do Algarve, P-8005-039 Faro, Portugal; and CCMAR, F.C.T., University of Algarve, P-8005-039 Faro, Portugal, e-mail: mcristi@ualg.pt
Amin Ismael: CCMAR and Department of Chemistry and Pharmacy, F.C.T., University of Algarve, P-8005-039 Faro, Portugal
Manabu Abe: Department of Chemistry, Graduate School of Science, Hiroshima University, Hiroshima, Japan

interesting coordination abilities and are thermally and photochemically much more stable than tetrazoles, although the saccharyl system is comparatively more difficult to functionalise [6, 7]. Taking advantage of the properties of both classes of heterocycles, we designed new scaffolds, termed as tetrazole-saccharinates (Scheme 1), with the aim of exploring their applications as multidentate nitrogen ligands. In recent years we prepared a representative library of tetrazole-saccharinates and investigated their structure in detail, prior to exploring their reactivity and applications [8–10].
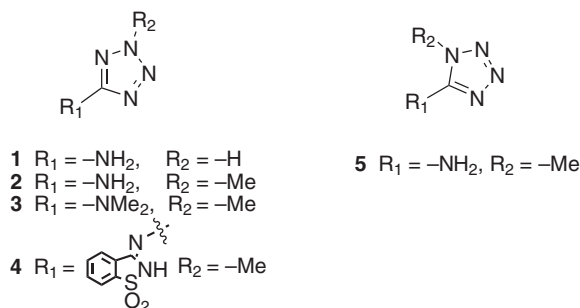
An investigation on the chelating ability of the new compounds revealed that selected N-linked tetrazole-saccharinates (Scheme 1; X = −NH− or −N=) exhibit strong binding selectivity to copper ions [11]. This property was considered of interest for therapeutic applications [12], mainly because of the recent findings that link elevated levels of copper to cancer progression [13, 14], boosting the interest in selective copper chelators [12, 15, 16]. The copper complexes prepared from selected N-linked tetrazole-saccharinates were tested *in vitro* against cancer cell lines and have shown a considerable increase in cytotoxicity against tumoral cells, compared to the corresponding nontoxic ligands [11]. Also, in a different line of investigation, two mononuclear copper (II) and cobalt (II) complexes based on the tetrazole-saccharinate ligand **4** (Scheme 2) were used as effective catalysts for selective oxidation of diverse secondary alcohols [17], while the ligand **4** alone proved effective as organo-catalyst for the oxidation of benzyl alcohols [18].

Despite the promising properties observed for these new tetrazole-saccharinate ligands, the tetrazole ring is known to undergo easy cleavage, induced thermally or photochemically [19–21]. Thus, when considering the applications of tetrazole-saccharinates, the low stability of this heterocycle steams as a concern. In this context we considered relevant to investigate the photochemistry of tetrazole-saccharinates, as the electron withdrawing saccharyl system, known to be relatively photostable, will probably affect the photostability of the tetrazole moiety [10].

Here we report the UV-induced photochemistry of monomeric 3-(2-methyl-(2H)-tetrazole-5-amino)-1,2-benzisothiazole 1,1-dioxide **4** (herein termed as 2-methyl-(2H)-tetrazole-5-amino-saccharinate, **2MTS**) isolated in solid argon. Compound **4** is one of our most promising ligands, since it proved to be nontoxic and selective towards Cu (II) and could be developed in the context of a new anti-tumor therapeutic approach based on selective copper chelation [11]. The matrix photochemistry of **4** is compared with that
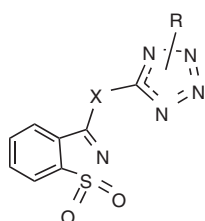
Scheme 1: Structural representation of the tetrazole-saccharinate chemotype.

1 R_1 = −NH$_2$, R_2 = −H
2 R_1 = −NH$_2$, R_2 = −Me
3 R_1 = −NMe$_2$, R_2 = −Me

5 R_1 = −NH$_2$, R_2 = −Me

4 R_1 = [structure] R_2 = −Me

Scheme 2: Structural representation of 5-aminotetrazoles with relevance to our investigation. Compounds **2**, **4** and **5** are the most important for the present study.

of other 5-aminotetrazole derivatives (Scheme 2), including 2-methyl-5-aminotetrazole **2**, used as building block for the preparation of the ligand **4**, and its isomer, 1-methyl-5-aminotetrazole **5**. It is worth noting that 5-aminotetrazoles are of interest as gas-generating compositions [22, 23], as high energy materials (e.g. as air-bag insufflators and as propellants components for missiles) [24–27] and, accordingly to recent findings, are being developed as powerful tools for proteome profiling in living cells [28–32]. Thus, a deeper investigation of the photochemistry of 5-aminotetrazoles and their derivatives is also especially relevant and timely.

As a whole, the results described herein, based on molecular orbital calculations and the matrix-isolation technique coupled to FTIR and EPR spectroscopies, pave the way towards a better elucidation of the mechanistic pathways followed by 5-aminotetrazoles upon UV-irradiation and of the effect of the ring substitution pattern on the photoreactivity of these compounds.

Results and discussion

Photochemistry of matrix-isolated 2-methyl-5-aminotetrazole-saccharinate (4)

As described in the Experimental Section, a sample of crystalline 2-methyl-(2*H*)-tetrazole-5-amino-saccharinate **4** was sublimated under reduced pressure (at ≈150 °C) and the vapors of the compound were co-deposited with argon (*ca.* 1:1000 molar ratio) onto a CsI substrate kept at 15 K. In previous studies, **4** was found to undergo a complete amino→imino tautomerization under the conditions described, where the amino-bridged tautomeric form existing in the crystalline phase of the compound was completely converted into the theoretically predicted most stable imino-bridged tautomer [9]. In this most stable tautomeric form, observed in the matrix isolation experiments, the labile hydrogen atom is connected to the saccharyl nitrogen and the two heterocyclic fragments are linked by an imino moiety in which the double-bond is established with the carbon atom belonging to the saccharyl fragment (see structure **4** in Scheme 3).

To investigate the photochemistry of **4**, the deposited matrix was irradiated with a tunable UV-laser source, starting at λ = 330 nm and gradually decreasing until λ = 222 nm (the shortest wavelength available in our experimental setup), with the sample being followed after each irradiation by recording its infrared spectrum. It was observed that irradiations at around λ ~ 290 nm and λ ~ 250 nm were the most effective in inducing changes in the spectrum of **4**.
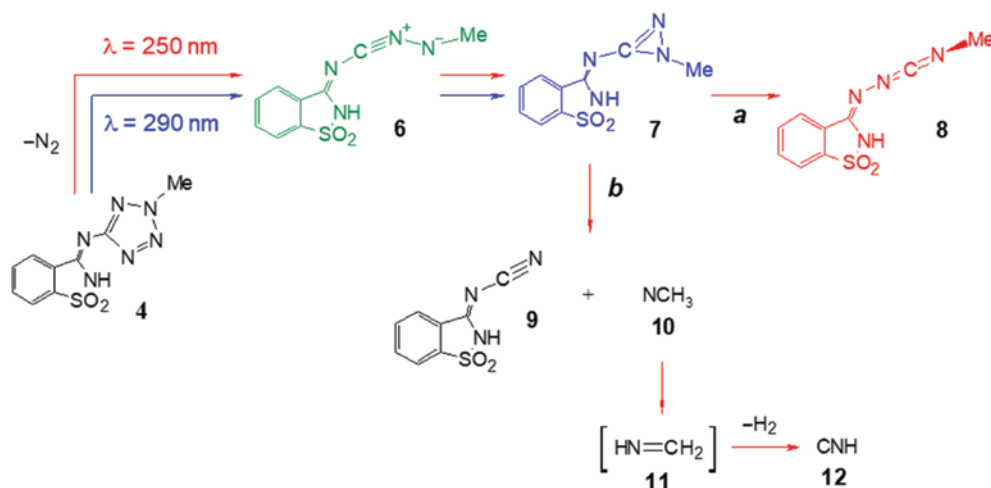
Scheme 3: Proposed reaction pathways resulting from irradiation of monomeric **4** isolated in solid argon, at λ = 290 nm (blue) and at λ = 250 nm (red).

Irradiations at $\lambda = 290$ nm, during up to 100 min., resulted in a decrease in the intensity of the bands due to **4** (indicating that the compound was being consumed) and, simultaneously, in a continuous increase of a distinctive absorption band at around 1680 cm^{-1}. Further irradiations of this same matrix at $\lambda = 250$ nm resulted in several new bands, with complete consumption of the reagent **4** after 10 min. of irradiation. Figure 1 presents the spectral changes in the range 2300–1700 cm^{-1}: (i) after 100 min. of irradiation at $\lambda = 290$ nm, when around 60 % of **4** was consumed and a chemical species, with a characteristic absorption at 1680 cm^{-1}, was produced, which could be identified as the 1H-diazirene **7** (see Scheme 3); (ii) after 5 and 10 min. of irradiation at $\lambda = 250$ nm, subsequent to the irradiation at $\lambda = 290$ nm, showing bands due to the different photoproducts generated at this wavelength. As reported for the photochemistry of an S-linked 1-methyltetrazole-saccharinate [10], the presence of the saccharyl ring, which seems to be unaffected by irradiation under the experimental conditions used, results in extensive overlap of the bands of **4** with those of the photoproducts, especially in the low-frequency spectral range (below 1700 cm^{-1}), hampering the interpretation of the data based on the low frequency spectral region. However, the most characteristic bands of these photoproducts are expected to appear in the clean 2300–1700 cm^{-1} spectroscopic window.

As it can be observed in Fig. 1, it is clear that in the 2300–1700 cm^{-1} spectral range no other bands increased besides the distinctive 1680 cm^{-1} absorption due to the diazirene **7**, even after 100 min. of irradiation at $\lambda = 290$ nm. Subsequent irradiation of the same matrix at $\lambda = 250$ nm resulted in a fast consumption of both the reactant **4** (see absorption at 1662 cm^{-1}) and the diazirene **7** while, simultaneously, several new bands (2263, 2138, 2118, 2050 cm^{-1}), due to other photoproduced species, appeared in the spectrum. The identification of the photoproducts corresponding to these characteristic absorption bands could be easily achieved by comparison with the reported results obtained for the photolysis of an S-linked tetrazole-saccharinate and the parent 2-methyl-5-aminotetrazole [10, 33]. The band at 2138 cm^{-1} was ascribed to the νNCN antisymmetric stretching of carbodiimide **8** (see Scheme 3), the band at 2263 cm^{-1} was ascribed to the νC≡N stretching of nitrile **9** and the band at 2050 cm^{-1} was ascribed to the νCN stretching of CNH **12**. The distinctive absorption at 2118 cm^{-1}, which increased during the first 5 min. of irradiation and then started decreasing with further irradiations at $\lambda = 250$ nm, was assigned to the νC=N stretching mode of the nitrile imine **6**, calculated at 2091 cm^{-1}. The spectral changes observed in the range 2300–2000 cm^{-1}, after 5 and 10 min of irradiation at $\lambda = 250$ nm, are shown in detail in Fig. 2. The calculated IR spectra for the proposed photoproducts are also shown in this figure, for comparison.

The mechanisms of fragmentation of tetrazoles remain under debate and the formation of nitrile imines from thermal and photochemical decomposition of tetrazoles has been subject of intense investigation over
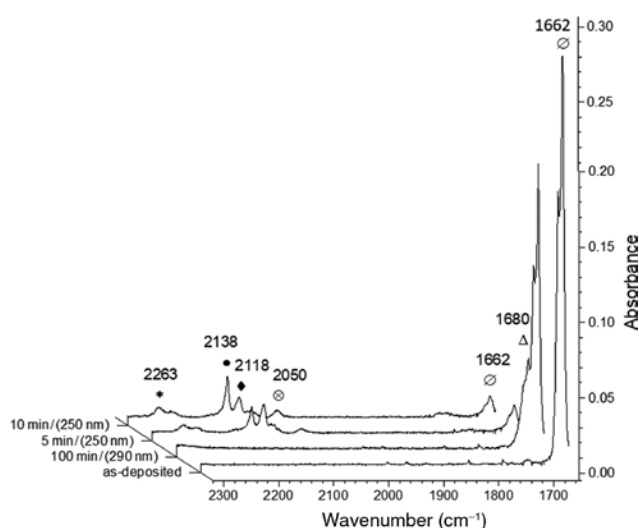

Fig. 1: Partial experimental IR spectra of compound **4**: for the freshly deposited matrix; after 100 min of irradiation at $\lambda = 290$ nm; and after 5 and 10 min of irradiation at $\lambda = 250$ nm, subsequent to the irradiation at $\lambda = 290$ nm.
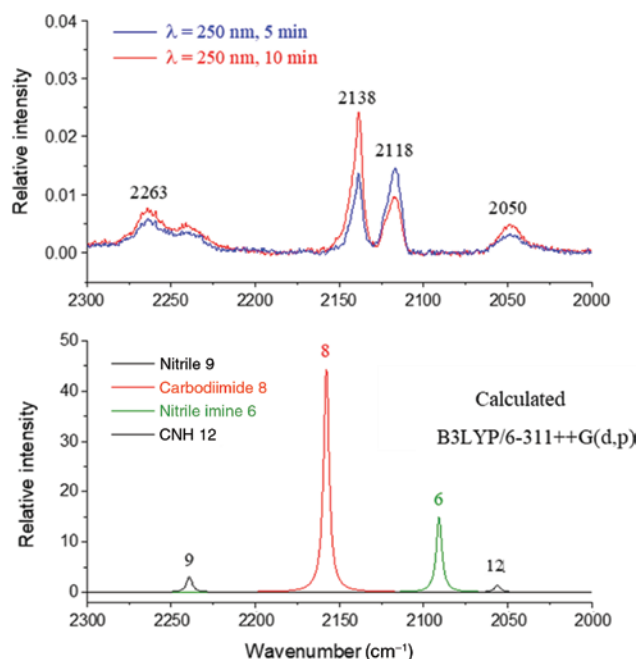
Fig. 2: (Top) IR spectrum in the 2300–2000 cm^{-1} spectral region for **4**, after irradiation of the matrix at $\lambda = 250$ nm for 5 min (red) and 10 min (blue), showing spectral changes upon irradiation; (bottom) theoretical spectra obtained for the observed photoproducts. Theoretical wavenumbers were scaled by a factor of 0.978, and bands were broadened using Lorentzian functions with fwhm equal to 4 cm^{-1}.

the last decades [19]. From the very first studies [32], it was postulated that the parent tetrazole in its gas phase most stable isomeric 2*H*-form, as well as 2-, 5- and 2,5-substituted tetrazoles, undergo fragmentation through formation of a nitrile imine intermediate that cyclizes to a 1*H*-diazirene, then leading to a final carbodiimide through rearrangement. However, this pattern of reactivity was demonstrated experimentally only very recently, during studies on the photochemistry of tetrazoles under low-temperature matrix isolation conditions [5, 13, 15, 21, 33, 35]. The observed outline of photo-fragmentation of **4** upon irradiation at $\lambda = 250$ nm follows this general pattern, which, as also found in other cases [10, 33], is accompanied by an additional reaction path involving as reactant the 1*H*-diazirene (see Scheme 3).

The initial step of the photochemistry of matrix-isolated **4** corresponds to selective photoinduced cleavage of the C$_5$–N$_4$ and N$_2$–N$_3$ bonds of the tetrazole ring, leading to extrusion of molecular nitrogen and production of nitrile imine **6**, which reached its maximum amount after the first 5 min. of irradiation at $\lambda = 250$ nm, and then was gradually consumed with increased irradiation times (see band 2118 cm^{-1} in Fig. 2; blue and red lines represent 5 min and 10 min of irradiation at $\lambda = 250$ nm, respectively), generating the 1*H*-diazirene **7** through a ring closing process.

It shall be noticed that, as mentioned above, upon irradiation of **4** at $\lambda = 290$ nm, the diazirene **7** was observed as the sole photoproduct. Although around 40 % of **4** remained after 100 min. of irradiation, suggesting that the efficiency of the reaction is rather low at this wavelength, it should be noticed that the capture of antiaromatic (i.e. 4π systems) structures such as **7** proved to be quite challenging, and has only been observed in rare cases, mostly upon isolation in cryogenic matrices [10, 33, 35–37]. Nevertheless, under the experimental conditions used, the antiaromatic three membered ring **7** could indeed be generated as the sole photoproduct and was found to be photostable. This result is even more remarkable because, contrarily to what is observed in this case, the diazirene derivative of 2-methyl-5-aminotetrazole was found to react upon irradiation at 325 nm [33]. On the other hand, the observed photostability of the antiaromatic three membered diazirene **7** follows the trend observed for a previously studied *S*-linked tetrazole-saccharinate [10], and appears to be a common phenomenon on this type of conjugates, probably induced by the stabilizing effect of the electron-withdrawing saccharyl moiety.

It is also interesting to note that during the irradiation experiments performed at 290 nm no spectroscopic evidence of any intermediate from **4** to the diazirene **7** was found, in particular no bands ascribable to nitrile imine **6**, which is observed upon irradiation at $\lambda = 250$ nm. This may be explained considering that the longer wavelength of excitation ($\lambda = 290$ nm), being closer to the absorbance maximum of the expected preceding nitrile imine **6** [38], facilitates its fast photoconversion into the diazirene **7**.

Upon irradiation at $\lambda = 250$ nm, the diazirene **7** undergoes subsequent photoconversion into carbodiimide **8** (pathway *a* in Scheme 3), in a process that will be discussed in more detail below. A second pathway was also perceived, pathway *b*, involving concomitant decomposition of the diazirene **7** and formation of nitrile **9** and CNH **12**.

Concerning pathway *b*, it should be noticed that the formation of nitrile **9** could in principle result either from (i) the cleavage of the C_5-N_4 and N_1-N_2 bonds of the tetrazole ring of **4**, generating the nitrile **9** and methyl azide, or from (ii) cleavage of the diazirene ring **7**, generating nitrile **9** and methyl nitrene **10**, the latter undergoing subsequent isomerization to methylenimine **11**, from which isocyanic acid (CNH) can be produced [39, 40]. However, formation of nitrile **9** *via* cleavage of the tetrazole ring can be ruled out, since no evidence of the intense νNNN antisymmetric mode of methyl azide could be found [40]. On the other hand, isocyanic acid was identified beyond doubt [39] and its formation from methylenimine **11** is expected based on the available knowledge regarding the photochemistry of this last compound [39, 40]. This mechanistic proposal is also supported by the results gathered from the photochemical investigation of the matrix-isolated parent 2-methyl-5-aminotetrazole **2**, which included EPR measurements, enabling the identification of methyl nitrene **10** (as described in detail below).

Effect of the saccharyl system on the photochemistry of 5-aminotetrazole derivatives

The present study revealed that photolysis of **4** results in a selective fragmentation of the tetrazole ring, while the saccharyl system seems to be completely photostable under the conditions used. As such, comparison of the photochemistry of **4** with that reported for the parent 2-methyl-5-aminotetrazole **2** [33] may be viewed as an efficient approach to support the interpretation of the present spectroscopic data, and to evaluate the photochemical stability induced by the electron withdrawing saccharyl system into the photolabile tetrazole.

The photochemistry of **4**, isolated in solid argon at 15 K, was investigated under similar conditions to those used for the parent tetrazole **2**. Irradiation was performed with a tunable laser at $\lambda = 250$ nm, with an output power of ~40 mW. It should be noted that both 5-aminotetrazole derivatives **2** and **4** show an absorption maximum at ~250 nm.

Comparison of the photochemistry of the conjugate **4** with that of the parent 2-methyl-5-aminotetrazole **2**, in the same experimental conditions, revealed that the reaction pathways and obtained photoproducts are equivalent for both compounds (Scheme 4). However, kinetic studies on the photodegradation of
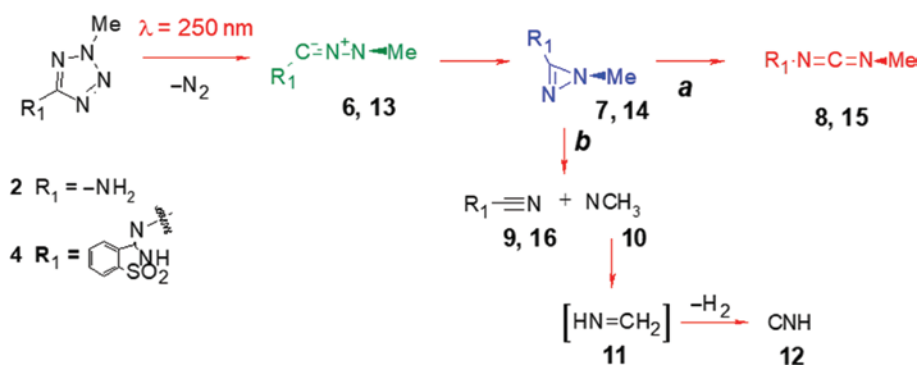
Scheme 4: Proposed reaction pathways resulting from irradiation of a matrix containing monomeric **2** or **4**, isolated in solid argon (15 K).

both compounds unfolded interesting differences in the kinetic profiles. Photolysis of matrix-isolated **2** at $\lambda = 250$ nm (~40 mW) generated the corresponding nitrile imine **13** in a maximal amount after 2 s of irradiation, which was totally consumed after 4 min. of irradiation. Also, *ca.* 50 % of the initial compound **2** was consumed after 4 s of irradiation [33]. On the other hand, photolysis of **4** under the same conditions ($\lambda = 250$ nm, ~40 mW) generated the corresponding nitrile imine **6** in a maximal amount after 5 min. of irradiation, and only after 60 min. of irradiation the nitrile imine was completely consumed. Moreover, *ca.* 50 % of the initial **4** was consumed only after 2 min. of irradiation. These results suggest that the saccharyl system increases the photostability of the tetrazole ring and also of the nitrile imine intermediate by more than 20×, compared to parent tetrazole **2**. These results are in keeping with the above noticed stabilization of the diazirene formed from **4** in result of the presence of the saccharyl substituent.

Mechanistic discussion of the photochemistry of matrix-isolated 1-methyl-tetrazole (5) and 2-methyl-tetrazole (2)

The general pattern of photoreactivity of 2-, 5- and 2,5-substituted tetrazoles has been described above. For 1,5-disubstituted tetrazoles, earlier studies [34, 38] postulated direct formation of the carbodiimide through an imidoylnitrene intermediate (see Fig. 3). In addition, more recent investigations demonstrated that 1*H*-diazirenes are common intermediates on the photochemistry of both 1,5- and 2,5-disubstituted tetrazoles [33].

During a study on the photochemistry of 5-methyl-tetrazole, Nunes et al. [35] have shown that 1*H*-diazirenes exhibit a close structural relation to imidoylnitrenes. Indeed, geometry optimization at the B3LYP/cc-pVTZ level on the triplet state of 5-methyl-1*H*-diazirene revealed convergence to the respective imidoylnitrene structure [35]. However, these imidoylnitrenes were only observed using internal or external traps [36, 37], since in the absence of these traps the reactive singlet state imidoylnitrene shall promptly cyclize to the 1*H*-diazirene or undergo a Wolff-type rearrangement into carbodiimide [41]. Recent studies on the photolysis of matrix-isolated tetrazoles allowed to identify several isomers formed from elimination
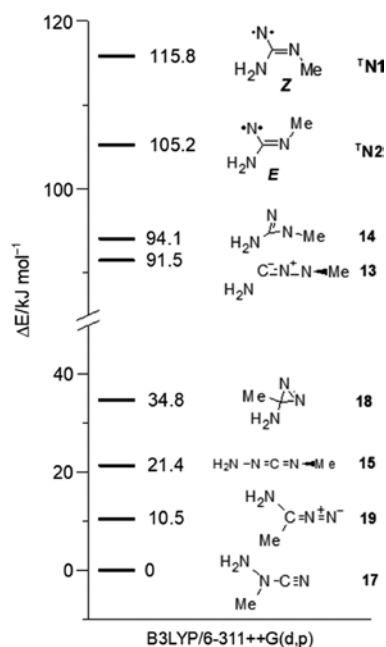

Fig. 3: Energies of eight C2H5N3 isomers calculated at the B3LYP/6-311++G(d,p) level (with zero-point energy correction included). The energies (in kJ mol⁻¹) are relative to the most stable isomer. For imidoylnitrene structures ^TN1 and ^TN2 the calculated energies correspond to the optimized triplet state geometries.

of molecular nitrogen, but attempts to trap the putative imidoylnitrene intermediates were unsuccessful [35, 42].

Following the reactivity patterns described above, two important observations result from recent studies regarding the effect of the ring substitution outline on the photofragmentation pathways of 5-amino-tetrazoles [33]: (i) the 1*H*-diazirene was observed as a common intermediate from photolysis of both 1-methyl- and 2-methyl-5-aminotetrazole, subsequently isomerizing to carbodiimide as final photoproduct; (ii) upon irradiation at short wavelengths (222 nm), an amino cyanamide was obtained, together with the 1*H*-diazirene and carbodiimide, from photolysis of 1-methyl-5-aminotetrazole, unraveling a new reaction pathway; this cyanamide isomerizes to the carbodiimide upon irradiation at longer wavelengths (325 nm).

In order to deepen our understanding of the effect of the ring substitution pattern on the mechanistic pathways followed by 5-aminotetrazole derivatives, further studies were undertaken. The $C_2H_5N_3$ isomers were calculated at the B3LYP/6-311++G(d,p) level and the structures are represented in Fig. 3. The calculated energies indicate that 1*H*-diazirene (**14** in Fig. 3) is the most energetic species in the singlet state; ~22 and ~11 kJ mol^{-1} below the imidoylnitrene triplet states ^{T}**N1** and ^{T}**N2**, respectively. The high energetic character of **14**, 94.1 kJ mol^{-1} above the amino cyanamide **17** (calculated as the most stable isomer in the singlet state potential energy surface), is conceivably due to both ring strain and antiaromatic destabilization. The observed trends for these isomeric species are similar to the trends found in calculations for $H_4C_2N_2$ and H_2CN_2 isomers, which can be formed from the photolysis of 5-methyl-tetrazole and of the parent unsubstituted tetra-zole, respectively [35, 42]. The optimized isomeric form *E* of triplet imidoylnitrene (^{T}**N2**) is more stable than form *Z* (^{T}**N1**) by ~10 kJ mol^{-1}.

In Scheme 5, a mechanistic proposal for the photochemical transformations of **5** and **2** isomers is presented, which is also in agreement with the observed photochemistry of **4**, described above. This mechanism considers as pivotal intermediate the highly reactive open-shell singlet state imidoylnitrene species, ^{s}**N**.
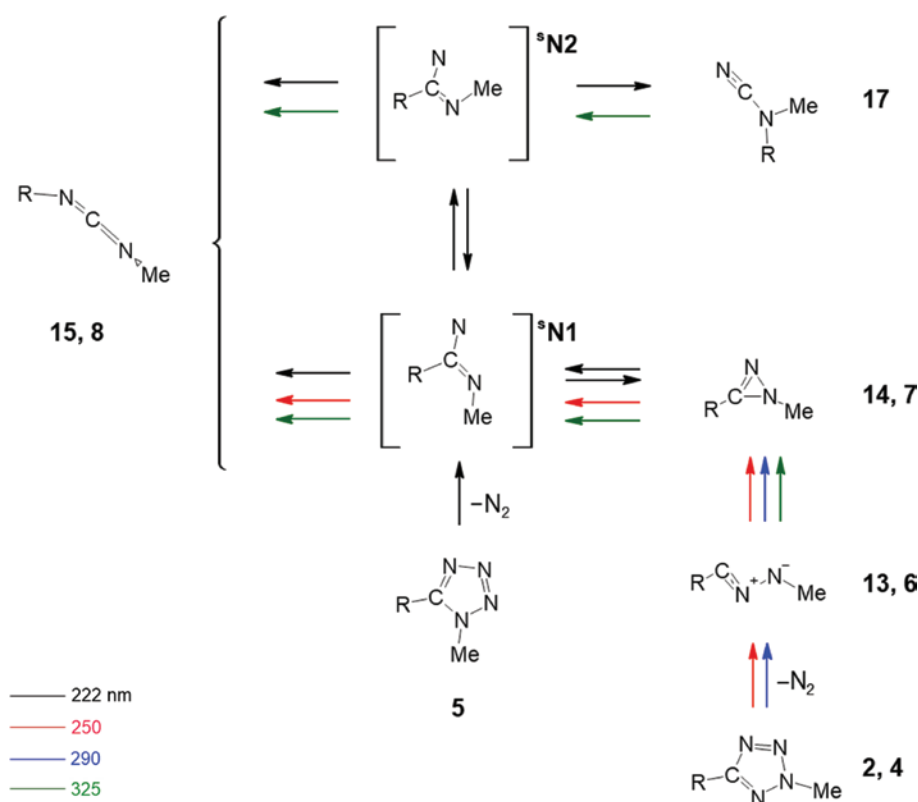
Scheme 5: Representation of the mechanistic proposal for the UV-induced photochemical pathways of **2**, **4** and **5**. The pathway *b* of Schemes 3 and 4 is not represented in this scheme for better reading of the picture.

Structurally, ^sN can be visualized as delocalized resonance structures with some biradical character at the two nitrogen atoms, and a central CN bond with appreciable double bond character [43–45].

As reported before [33], the $\lambda = 250$ nm photolysis of **2** results in the cleavage of the tetrazole ring, with initial formation of nitrile imine **13** that develops to diazirene **14**. This last one is expected to generate the imidoylnitrene in the geometrically most accessible Z isomeric form $^SN1$, through ring opening. The reactive Z-$^sN1$ species can then rearrange to the observed carbodiimide **15**, *via* a direct R-group 1,2-shift (R = amino group) from the carbon of the imidoylnitrene to the sterically accessible nitrene moiety (in this isomeric form of the imidoylnitrene, the methyl substituent precludes the 1,2-shift to the methyl-substituted nitrogen). Several thermal and photochemical reactions of tetrazoles involving imidoylnitrenes' rearrangements were postulated based on this 1,2-shift [19]. Indeed, imidoylnitrenes are aza analogs of vinylnitrenes and acylnitrenes, thus these reactions can be expected to follow the same Wolff-type rearrangement to carbodiimides [41].

Compared to **2**, the first step of the photolysis of **5** leads to a different product, though in both cases cleavage of the tetrazole ring, with extrusion of molecular nitrogen, takes place. In the case of **5**, this process directly generates the postulated imidoylnitrene intermediate Z-$^sN1$. Once formed, Z-$^sN1$ can undergo the above mentioned Wolff-type rearrangement to carbodiimide **15**, or collapse to give the $1H$-diazirene **14**, which are then common photoproducts from photolysis of both 5-aminotetrazole isomers **2** and **5**. The observation of the cyanamide **17** photoproduct during the short wavelength irradiation (222 nm) [33] of **5** can be explained by considering that at this irradiation wavelength the channel for photoisomerization between Z and E forms of the imidoylnitrene is accessible. In the E imidoylnitrene isomeric form $^sN2$, the methyl substituent is no longer blocking the 1,2-shift from the amino group to the methyl-substituted nitrogen, thus allowing generation of the cyanamide **17** by a mechanism similar to that discussed above leading to rearrangement of the imidoylnitrene into the carbodiimide **15**.

As mentioned above, it was also shown [33] that upon subsequent irradiation at 325 nm of a photolysed argon matrix of **5**, the formed cyanamide **17** (and also the diazirene **14**) converts into the carbodiimide **15**, a result that is also explained by the mechanism shown in Scheme 4 and involves participation of
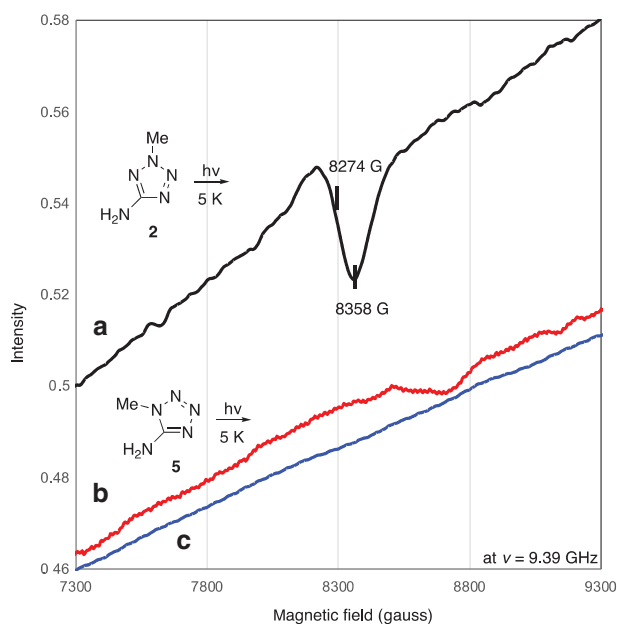

Fig. 4: EPR spectra obtained in the photolysis of aminotetrazoles. (a) After irradiation of compound **2** for 60 min at 266 nm at 5 K in MTHF, assigned to the X_2 (8274 G) and Y_2 (8358 G) transition of methylnitrene **10** ($|D/hc| = 1.61$ cm^{-1} and $|E/hc| = 0.0015$ cm^{-1}) at the resonance frequency of 9.39 GHz. (b) After 11 h irradiation of compound **5** using Xenon lamp (>220 nm) at 5 K. (c) After 11 h irradiation of compound **5** at 266 nm at 5 K in MeOH.

the imidoylnitrene intermediate. Recently, Abe et al. [46] reported the formation of an imidoyl nitrene from photolysis of 1-methyl-5-phenyl-tetrazole, which was observed by EPR (electron paramagnetic resonance) spectroscopy.

We performed EPR (electron paramagnetic resonance) spectroscopy for the photolysis of **5** and **2** in cryogenic conditions, aimed at trapping and identifying putative nitrene species. According to the reported data [47], we can expect to observe different EPR signatures for nitrenes and diradicals and they can be distinguished by EPR, where nitrenes give rise to transitions at high field (typically ~7000 G) and zero-field splitting parameters D of around 1 cm^{-1}, whereas diradicals resonate at much lower field (typically ~3000 G) and show much smaller D values.

In these EPR studies, ca. 50 mM 2-methyltetrahydrofuran (MTHF) solution of **2** and the suspension of **5** were degassed under high vacuum at 1.0×10^{-2} Pa and sealed under the vacuum conditions, respectively. The solubility of tetrazole **5** was quite low. The EPR sample of **2** was placed in the EPR cavity, cooled to 5 K, and then irradiated at 266 nm (~10 mJ). After irradiation of compound **2** under these conditions for 60 min., the EPR spectrum of photolyzed **2** evidenced a signal at around 8280 G, at the resonance frequency of 9.39 GHz (Fig. 4a), which was identified as methyl nitrene **10**, with $|D/hc| = 1.61$ cm^{-1} and $|E/hc| = 0.0015$ cm^{-1}, which are consistent with reported values in organic matrix [48]. This observation brings further support to our proposal that nitriles **9** and **16** result from photolysis of diazirenes **7** and **14**, respectively (see Schemes 2 and 3), with concomitant formation of methyl nitrene **10** that rearranges to methylene imine **11**, then affording isocyanic acid **12**.

For compound **5**, the irradiation with a broadband Xe-light source had to proceed for 11 h until a very weak signal could be observed, at ~8500 G, also ascribed to a triplet nitrene (Fig. 4b). It should be noted that the irradiation wavelength ($\lambda = 266$ nm) is far from the maximum absorption (~222 nm) observed for **5**, and even the Xe-lamp has a very weak light intensity below ~250 nm. In addition, the solubility of tetrazole **5** proved to be quite low, as mentioned above.

In consonance with the reported information, these EPR results seem to be the first direct observation of the postulated methylnitrene intermediate from the photolysis of diazirenes. Unfortunately, we could not observe evidence of the postulated diradical imidoyl nitrene ^{s}**N1** which, according to the reported data, can be expected to be mixed with the strong signals at ~3500 G, which were derived from doublet impurities.

Conclusion

The potential applications of 2-methyl-(2*H*)-tetrazole-5-amino-saccharinate (**2MTS; 4**, Scheme 2) in catalysis and in chelant-based chemotherapy stimulated the study of its photostability. The photochemistry of monomeric **2MTS** was investigated and the results were compared with those obtained for other 5-aminotetrazole derivatives (Scheme 2), including 2-methyl-(2*H*)-tetrazole-5-amine (**2MT; 2**) used as building block for its synthesis. The compounds were isolated in solid argon (15 K) and the matrix was subjected to *in situ* narrowband UV excitation at different wavelengths, which proved to induce selective photochemical transformations of the reactants and also of the initially formed photoproducts. The progress of the reactions was followed by infrared spectroscopy, supported by quantum chemical calculations. Irradiation of matrix-isolated **2MTS** at $\lambda = 290$ nm for 100 min resulted in consumption of around 60 % of the reactant. Under these conditions, the sole product observed was the antiaromatic 1*H*-diazirene **7** (Scheme 3), which remained photostable. On the other hand, irradiation of matrix-isolated **2MTS** at $\lambda = 250$ nm led to a faster consumption of the reagent, with formation of nitrile imine **6**, which rapidly cyclized to diazirene **7**. At $\lambda = 250$ nm diazirene **7** was found to be unstable, reacting through two concomitant reaction pathways: (a) photoisomerization to photostable carbodiimide **8**; (b) photodecomposition, leading to stable nitrile **9** and isocyanic acid CNH **12**, which most probably derives from methyl nitrene. Noteworthy, the saccharyl system remained stable under both irradiation conditions, the photodegradation of **2MTS** relying exclusively on extrusion of N$_2$ from the tetrazolyl ring. The photodegradation pattern of **2MTS** proved to be similar to that of its parent **2MT**, although the reaction was about 20 times slower. In fact, our studies have clearly demonstrated the stabilizing effect of the saccharyl

system on the photostability of the tetrazolyl moiety, in **2MTS**, this effect also extending to the nitrile imine intermediate **6** and to the antiaromatic 1*H*-diazirene **7**, found to be photostable at 290 nm, in contrast to the 1*H*-diazirene derived from 2-methyl-5-aminotetrazole, which was found to react upon irradiation at 325 nm. A similar photo-stabilizing effect induced by the electron-withdrawing saccharyl moiety was observed during a previous study of the photochemistry of a *S*-linked tetrazole-saccharinate [10].

The photochemistries of **2MT** (2-methyl-(1*H*)-tetrazole-5-amine) and of its isomer **1MT** (1-methyl-(1*H*)-tetrazole-5-amine) were revisited in order to further understand the effect of the ring substitution pattern on the mechanistic pathways followed by 5-aminotetrazoles. Our previous results [10, 33] had shown that: (i) 1*H*-diazirene **14** is a common intermediate from photolysis of both **1MT** and **2MT**; (ii) irradiation of **1MT** at short wavelengths (222 nm) also affords the amino cyanamide **17** ($H_2N-N(CH_3)-C{\equiv}N$), which isomerizes to the carbodiimide **15** upon irradiation at longer wavelengths (325 nm); (iii) formation of the amino cyanamide **17** is only observed from the photocleavage of **1MT**, whereas formation of the nitrile imine **13** ($H_2N-C^-=N^+=N-CH_3$) is only obtained from photolysis of **2MT**. Considering that the observed photoproduct selectivity may be related to the structure of the $C_2H_5N_3$ isomers formed after extrusion of molecular nitrogen from **1MT** and **2MT**, calculations were performed at the B3LYP/6-311++G(d,p) level and EPR studies on the photolysis of both compounds were also conducted. Scheme 5 shows the energy trends for the isomeric $C_2H_5N_3$ species, according to the calculations. Analysis of these data indicated that 1*H*-diazirene **14** is the most energetic species in the singlet state, 94.1 kJ mol^{-1} above the amino cyanamide **17** and only ~22 and ~11 kJ mol^{-1} below the imidoylnitrene triplet states ^{T}**N1** and ^{T}**N2**, respectively (Scheme 5). The optimized isomeric form *E* of triplet imidoylnitrene (^{T}**N2**) is more stable than form *Z* (^{T}**N1**) by ~ 10 kJ mol^{-1}.

Considering all data available, we proposed mechanisms for the photochemical transformations of **1MT** (**5**), **2MT** (**2**) and **2MTS** (**4**), further clarifying the pathways followed by 1,5-substituted and 2,5-substituted tetrazoles under UV-induced excitation (Scheme 5). We postulate a singlet state imidoylnitrene species, ^{s}**N1**, as common intermediate, which undergoes a Wolff-type isomerization to afford a stable carbodiimide (**15**, **8**). For 1,5-substituted tetrazole (**5**) the pivotal imidoylnitrene species may be acceded directly upon photo-extrusion of N$_2$, whereas for 2,5-substituted tetrazoles (**2,4**) the loss of N$_2$ originates a nitrilimine (**13**, **6**), which cyclizes to a diazirene (**14**, **7**), then leading to the proposed pivotal singlet state imidoylnitrene species ^{s}**N1**. We believe that the selective formation of the cyanamide **17** from photolysis of **5** is due to the short wavelength irradiation (222 nm) required for photolysis of this compound, which also renders accessible the channel for photoisomerization between *Z* and *E* forms of the imidoylnitrene. In the *E*-imidoylnitrene isomeric form ^{s}**N2**, the methyl substituent is no longer blocking the 1,2-shift from the amino group to the methyl-substituted nitrogen, thus allowing generation of the cyanamide through a Wolff-type isomerization.

The EPR studies on the photolysis of compounds **2** and **5** enabled the detection of methyl nitrene **10**, supporting our proposal that photostable nitriles (9, 16) arise from photodecomposition of diazirenes (**7**, **14**), together with methyl nitrene, which further reacts to give isocyanic acid (Scheme 4; pathway **b**).

Experimental section

General information

All chemicals were of analytical grade and were used as purchased. Solvents for extraction were of technical grade. When required, solvents were freshly distilled from appropriate drying agents before use. Melting points were recorded and are uncorrected. Mass spectra were obtained by electron ionization (EI) at 70 eV. NMR (400 MHz) spectra were measured using TMS as the internal reference ($\delta = 0.0$ ppm).

Preparation of compounds. Methyltetrazole-5-amines (**2**, **5**) were prepared from commercially available 5-aminotetrazole monohydrate through methylation, as previously described [49].

1-Methyl-(1*H*)-tetrazole-5-amine (1TMS; 5): colorless needles (6.1 g; 51 % yield), m.p. 220–221 °C (lit, 220 °C [49]); ^{1}H NMR (400 MHz, CDCl$_3$): δ 4.15 (3H, s); MS (EI): *m/z* 99 [M]$^+$.

2-Methyl-(2H)-tetrazole-5-amine (2MT; 2): colorless needles (3.0 g, 25 % yield), m.p. 104–105 °C (lit, 104 °C [49]); ^{1}H NMR (400 MHz, CDCl$_3$): δ 3.32 (3H, s); MS (EI): m/z 99 [M]$^+$.

2-Methyl-(2H)-tetrazole-5-amino-saccharinate (2MTS; 4): obtained through convergent synthesis, by coupling 2-methyl-(2H)-tetrazol-5-amine (0.25 g; 2.56 mmol) with freshly prepared 3-chloro-1,2-benziso-thiazole 1,1-dioxide (0.53 g, 2.56 mmol) in dry THF (20 mL). The mixture was stirred at 60 °C for 24 h under a nitrogen atmosphere. Colorless crystals (0.48 g; 72 % yield), m.p. 284–286 °C (lit, 285–286 °C [47]), ^{1}H NMR (DMSO): δ 8.49–8.50 (m, 1H), 8.10–8.13 (m, 1H), 7.90–7.92 (m, 2H), 4.42 (s, 3H), MS (EI): m/z 250 [M$^+$].

3-Chloro-1,2-benzisothiazole-1,1-dioxide was obtained from saccharin (10.2 g; 56 mmol) and phosphorus pentachloride (14.0 g; 66 mmol) using an halogenation procedure reported previously [49]: colorless needles (7.00 g; 63 % yield); m.p. 143–145 °C; ^{1}H NMR (CDCl$_3$): δ 7.85 (4H, m, Ar-H); elemental analysis: C 41.5 %, H, 2.0 %, N, 6.9 % (found), C, 41.7 %, H, 2.0 %, N, 7.0 % (calculated for C$_7$H$_4$NO$_2$SCl); MS (EI): m/z 201 [M]$^+$

Matrix preparation, infrared spectroscopy

The matrix was prepared by codeposition of the matrix gas (argon, 99.9998 %, obtained from Air Liquid) and vapors of the tetrazole under analysis (**1a** or **1b**) produced by sublimation onto the cooled CsI substrate of the cryostat in a specially designed variable-temperature mini-oven assembled inside the cryostat. The cryogenic system was based on a closed-cycle helium refrigeration system with a DE-202A expander. The temperature of the CsI substrate during deposition was 15 K. The infrared spectrum of matrix-isolated compounds was obtained using a Fourier transform infrared spectrometer equipped with a deuterated triglycinesulfate (DTGS) detector and a Ge/KBr beam splitter with 0.5 cm^{-1} spectral resolution.

UV-laser irradiation experiments

The matrices were irradiated through the outer quartz window of the cryostat using a narrow band (fwhm ~0.2 cm^{-1}) with the frequency-doubled signal beam of a Quanta-Ray MOPO-SL pulsed optical parametric oscillator, pumped with a pulsed Nd:YAG laser (repetition rate = 10 Hz, pulse energy ≈1–5 mJ, duration = 10 ns). The UV light used to induce the initial photochemistry of **4** was selected according to the UV-vis spectrum obtained in ethanol at room temperature, which show absorption maxima at ~222 and ~248 nm.

Theoretical calculations

Quantum-chemical calculations were performed with density functional theory using the 6-311++G(d,p) basis set [50, 51] and the B3LYP functional [52, 53]. The optimization of geometries was followed by harmonic vibrational calculations undertaken at the same level of theory. The calculated harmonic vibrational frequencies were scaled by a factor of 0.968, obtained by least-squares linear fit of the experimental versus calculated frequencies of **4**. The calculated frequencies were then used to simulate the spectra using Lorentzian functions with fwhm equal to 4 cm^{-1} and to assist the analysis of the experimental spectra. All of the calculations were performed with the Gaussian 09 suite of programs [54].

EPR experiments

A 50 mM solution of **2** or **5** in anhydrous MTHF was degassed by three freeze/thaw cycles using diffusion and rotary pumps. The tube containing the solution was sealed after degassing and used for EPR spectroscopy measurements. The low temperature EPR spectra were recorded on a X-band Bruker E-500 using liquid helium cryostat.

References

[1] M. X. Li, Y. F. Zhang, X. He, X. M. Shi, Y. P. Wang, M. Shao, Z. X. Wang. *Cryst. Growth Des.* **16**, 2912 (2016).

[2] X. Wang, N. Li, A. Tian, J. Ying, T. Li, X. Lin, J. Luan, Y. Yang. *Inorg. Chem.* **53**, 7118 (2013).

[3] E. A. Popova, R. E. Trifonov, V. A. Ostrovskii. *Arkivoc* **2012**, 45 (2012).

[4] H. Zhao, Z.-R. R. Qu, R.-G. G. Xiong. *Chem. Soc. Rev.* **37**, 84 (2008).

[5] J. Roh, K. Vávrová, A. Hrabálek. *Eur. J. Org. Chem.* **31**, 6101 (2012).

[6] Z. Jakopin, M. S. Dolenc. *Curr. Med. Chem.* **17**, 651 (2010).

[7] E. J. Baran, V. T. Yilmaz. *Coord. Chem. Rev.* **250**, 1980 (2006).

[8] A. Gómez-Zavaglia, A. Ismael, L. I. L. Cabral, A. Kaczor, J. A. Paixão, R. Fausto, M. L. S. Cristiano. *J. Mol. Struct.* **1003**, 103 (2011).

[9] A. Ismael, A. Gómez-Zavaglia, A. Borba, M. L. S. Cristiano, R. Fausto. *J. Phys. Chem. A* **117**, 3190 (2013).

[10] A. Ismael, A. Borba, M. S. C. Henriques, J. A. Paixão, R. Fausto, M. L. S. Cristiano. *J. Org. Chem.* **80**, 392 (2015).

[11] A. Ismael, M. S. C. Henriques, C. F. S. Marques, M. J. Rodrigues, L. A. Barreira, J. A. Paixão, R. Fausto, M. L. S. Cristiano. *RSC Adv.* **6**, 71628 (2016).

[12] X. Ding, H. Xie, Y. J. Kang. *J. Nutr. Biochem.* **22**, 301 (2016).

[13] A. Gupte, R. Mumper. *J. Cancer Treat. Rev.* **35**, 32 (2009).

[14] K. Jomova, M. Valko. *Toxicology* **283**, 65 (2011).

[15] M. Fatfat, R. A. Merhi. O. Rahal, D. A. Stoyanovsky, A. Zaki, H. Haidar, V. E. Kagan, H. Gali-Muhtasib, K. Machaca. *BMC Cancer* **14**, 527 (2014).

[16] R. K. Blackman, K. Cheung-Ong, M. Gebbia, D. A. Proia, S. He, J. Kepros, A. Jonneaux, P. Marchetti, J. Kluza, P. E. Rao, Y. Wada, G. Giaever, C. Nislow. *PLoS One* **7**, e29798 (2012).

[17] L. M. T. Frija, E. C. B. A. Alegria, M. Sutradhar, M. L. S. Cristiano, A. Ismael, M. N. Kopylovich, A. J. L. Pombeiro. *J. Mol. Catal. A Chem.* **425**, 283 (2016).

[18] L. M. T. Frija, M. L. Kuznetsov, B. G. M. Rocha, L. Cabral, M. L. S. Cristiano, M. N. Kopylovich, A. J. L. Pombeiro. *Mol. Catal.* **422**, 57 (2017).

[19] C. Wentrup. *Chem. Rev.* **117**, 4562 (2017).

[20] L. M. T. Frija, M. L. S. Cristiano, A. Gómez-Zavaglia, I. Reva, R. Fausto. *J. Photochem. Photobiol. C Photochem. Rev.* **18**, 71 (2014).

[21] L. M. T. Frija, A. Ismael, M. L. S. Cristiano. *Molecules* **15**, 3757 (2010).

[22] Y. Miyata, S. Date, K. Hasue. *Propell. Explos. Pyrotech.* **29**, 247 (2004).

[23] S. P. Burns, P. S. Khandhadia. Nonazide gas generant compositions. United States Patent US5872329 (1999).

[24] T. M. Klapötke, P. Mayer, A. Schulz, J. J. Weigand. *J. Am. Chem. Soc.* **127**, 2032 (2005).

[25] H. Xue, Y. Gao, B. Twamley, J. M. Shreeve. *Chem. Mater.* **17**, 191 (2005).

[26] D. Fischer, T. M. Klapötke, J. Stierstorfer. *Propell. Explos. Pyrotech.* **37**, 156 (2012).

[27] J. Stierstorfer, K. R. Tarantik, T. M. Klapötke. *Chemistry* **15**, 5775 (2009).

[28] C. P. Ramil, Q. Lin. *Curr. Opin. Chem. Biol.* **21**, 89 (2014).

[29] Z. Li, D. Wang, L. Li, S. Pan, Z. Na, C. Y. J. Tan, S. Q. Yao. *J. Am. Chem. Soc.* **136**, 9990 (2014).

[30] M. A. Tasdelen, Y. Yagci. *Angew. Chem. Int. Ed.* **52**, 5930 (2013).

[31] Z. Yu, T. Y. Ohulchanskyy, P. An, P. N. Prasad, Q. Lin. *J. Am. Chem. Soc.* **135**, 16766 (2013).

[32] H. Shi, C. J. Zhang, G. Y. J. Chen, S. Q. Yao. *J. Am. Chem. Soc.* **134**, 3001 (2012).

[33] A. Ismael, R. Fausto, M. L. S. Cristiano. *J. Org. Chem.* **81**, 11656 (2016).

[34] S. Fischer, C. Wentrup. *J. Chem. Soc. Chem. Commun.* **11**, 502 (1980).

[35] C. M. Nunes, C. Araujo-Andrade, R. Fausto, I. Reva. *J. Org. Chem.* **79**, 3641 (1914).

[36] G. Alcaraz, A. Baceiredo, M. Nieger, G. Bertrand. *J. Am. Chem. Soc.* **116**, 2159 (1994).

[37] F. L. Bach, J. Karliner, G. E. Van Lear. *J. Chem. Soc. D Chem. Commun.* **276**, 1110 (1969).

[38] D. Bégué, G. G. Qiao, C. Wentrup. *J. Am. Chem. Soc.* **134**, 5339 (2012).

[39] D. E. Milligan, M. E. Jacox. *J. Chem. Phys.* **39**, 712 (1963).

[40] D. E. Milligan. *J. Chem. Phys.* **35**, 1491 (1961).

[41] C. Wentrup. *Carbenes and Nitrenes in Heterocyclic Chemistry: Intramolecular Reactions*, (1981) Vol. 28.

[42] G. G. Maier, J. J. Eckwert, A. Bothur, H. P. Reisenauer, C. Schmidt. *Liebigs Ann.* **7**, 1041 (1996).

[43] R. A. Moss, M. Platz, M. Jones. *Reactive Intermediate Chemistry*, John Wiley and Sons, New York (2004).

[44] F. V. E. Scriven. *Azides and Nitrenes*, Academic Press, Indianapolis, IND (1984).

[45] E. G, Baskir, D. N. Platonov, Y. V. Tomilov, O. M. Nefedov. *Mendeleev Commun.* **24**, 197 (2014).

[46] M. Abe, D. Bégué, H. Santos-Silva, A. Dargelos, C. Wentrup. *Angew. Chem. Int. Ed.* **57**, 3212 (2018).

[47] C. Wentrup, D. Kvaskoff. *Aust. J. Chem.* **66**, 286 (2013).

[48] L. Barash, E. Wasserman, W. A. Yager. *J. Am. Chem. Soc.* **89**, 3931 (1967).

[49] A. Ismael, J. A. Paixão, R. Fausto, M. L. S. Cristiano. *J. Mol. Struct.* **1023**, 128 (2012).

[50] M. J. Frisch, J. A. Pople, J. S. Binkley. *J. Chem. Phys.* **80**, 3265 (1984).

[51] R. Krishnan, J. S. Binkley, R. Seeger, J. A. Pople. *J. Chem. Phys.* **72**, 650 (1980).

[52] P. M. W. Gill, B. G. Johnson, J. A. Pople, M. J. Frisch. *Chem. Phys. Lett.* **197**, 499 (1992).

[53] A. D. Becke. *Phys. Rev. A* **38**, 3098 (1988).

[54] M. J. Frisch, G. W. Trucks, H. B. Schlegel, G. E. Scuseria, M. A. Robb, J. R. Cheeseman, G. Scalmani, V. Barone, B. Mennucci, G. A. Petersson, H. Nakatsuji, M. Caricato, X. Li, H. P. Hratchian, A. F. Izmaylov, J. Bloino, G. Zheng, J. L. Sonnenberg, M. Hada, M. Ehara, K. Toyota, R. Fukuda, J. Hasegawa, M. Ishida, T. Nakajima, Y. Honda, O. Kitao, H. Nakai, T. Vreven, J. A. Montgomery, J. E. Peralta, F. Ogliaro, M. Bearpark, J. J. Heyd, E. Brothers, K. N. Kudin, V. N. Staroverov, R. Kobayashi, J. Normand, K. Raghavachari, A. Rendell, J. C. Burant, S. S. Iyengar, J. Tomasi, M. Cossi, N. Rega, J. M. Millam, M. Klene, J. E. Knox, J. B. Cross, V. Bakken, C. Adamo, J. Jaramillo, R. Gomperts, R. E. Stratmann, O. Yazyev, A. J. Austin, R. Cammi, C. Pomelli, J. W. Ochterski, R. L. Martin, K. Morokuma, V. G. Zakrzewski, G. A. Voth, P. Salvador, J. J. Dannenberg, S. Dapprich, A. D. Daniels, O. Farkas, J. B. Foresman, J. V. Ortiz, J. Cioslowski, D. J. Fox. *Gaussian 09, Revision A.02*, Gaussian, Inc., Wallingford, CT (2009).